



Citation: Mosheiff N, Ermentrout B, Huang C (2023) Chaotic dynamics in spatially distributed neuronal networks generate population-wide shared variability. PLoS Comput Biol 19(1): e1010843. https://doi.org/10.1371/journal.pcbi.1010843

Editor: Hugues Berry, Inria, FRANCE

Received: April 29, 2022

Accepted: December 26, 2022

Published: January 10, 2023

Copyright: © 2023 Mosheiff et al. This is an open access article distributed under the terms of the Creative Commons Attribution License, which permits unrestricted use, distribution, and reproduction in any medium, provided the original author and source are credited.

Data Availability Statement: All relevant data are within the paper and its <u>Supporting information</u> files

Funding: C.H. was supported by NIH grant R01NS121913 and the University of Pittsburgh. B. E. was partially supported by NSF DMS 1951099. The funders had no role in study design, data collection and analysis, decision to publish, or preparation of the manuscript.

Competing interests: The authors have declared that no competing interests exist.

RESEARCH ARTICLE

Chaotic dynamics in spatially distributed neuronal networks generate population-wide shared variability

Noga Mosheiff^{1,2}, Bard Ermentrout³, Chengcheng Huang^{1,2,3}*

- 1 Department of Neuroscience, University of Pittsburgh, Pittsburgh, Pennsylvania, United States of America, 2 Center for the Neural Basis of Cognition, Pittsburgh, Pennsylvania, United States of America, 3 Department of Mathematics, University of Pittsburgh, Pittsburgh, Pennsylvania, United States of America
- * huangc@pitt.edu

Abstract

Neural activity in the cortex is highly variable in response to repeated stimuli. Population recordings across the cortex demonstrate that the variability of neuronal responses is shared among large groups of neurons and concentrates in a low dimensional space. However, the source of the population-wide shared variability is unknown. In this work, we analyzed the dynamical regimes of spatially distributed networks of excitatory and inhibitory neurons. We found chaotic spatiotemporal dynamics in networks with similar excitatory and inhibitory projection widths, an anatomical feature of the cortex. The chaotic solutions contain broadband frequency power in rate variability and have distance-dependent and low-dimensional correlations, in agreement with experimental findings. In addition, rate chaos can be induced by globally correlated noisy inputs. These results suggest that spatiotemporal chaos in cortical networks can explain the shared variability observed in neuronal population responses.

Author summary

Cortical neurons exhibit highly variable spatiotemporal activity patterns, even in the presence of strong sensory stimuli. The patterns of population responses also vary depending on animal's brain state and behavioral context. Understanding the dynamical properties of cortical circuit is critical to understanding network's responses to stimulus inputs. Previous models have proposed that neural variability can be generated through chaotic neural dynamics in cortical circuits. However, these models fail to capture the statistical features of the shared variability in population activity patterns observed in experiments. In this work, we systematically analyze the dynamical regimes of spatially distributed neuronal networks. We discover spatiotemporal chaos that produces correlated response patterns in neural population activity, consistent with cortical recordings. Interestingly, we find chaos in networks where the excitatory and inhibitory neurons have similar spatial spreads of connections, which is an anatomical feature of sensory cortex. We further show that chaotic activity can be induced when the network is driven by correlated noisy inputs,

which can explain the prevalence of large-scale shared variability observed in cortex. Our work expands our mechanistic understanding of neural dynamics in cortical circuit models.

Introduction

A defining feature of cortical neural responses is that they are highly variable. The variability is reflected at multiple scales of neural recordings, from irregular inter-spike intervals in spike trains of individual neurons [1, 2] to spatiotemporal patterns in mesoscopic neural activity measured with voltage sensitive dye imaging [3] and local field potentials [4], to whole brain signals such as the electroencephalography [5]. Changes in neural variability reflect fluctuations in the brain state and are closely related to behavioral performance [5–8]. Therefore, understanding the circuit mechanisms that generate neural variability is critical for elucidating the neural basis of behavior.

Previous models have proposed that chaotic neural dynamics can be a substantial local source of neural variability in cortical circuits [9–11]. Variable neural responses can be intrinsically generated through strong interactions between the excitatory and inhibitory neurons. Intriguingly, neuronal networks with chaotic dynamics have been shown to demonstrate high computational capabilities because of their rich reservoir of internal dynamics that can be utilized for complex computations and efficient training [12–16].

However, previous models with unstructured random connectivity produce chaotic response in individual neurons that is uncorrelated with other neurons in the network. In contrast, numerous datasets of cortical recordings have revealed that cortical neurons are on average positively correlated [17]. The correlation between a pair of neurons depends on many factors, such as the cortical distance between them and their tuning similarity [18–20]. Moreover, the variability shared among a neuron population has been found to be low dimensional, meaning that the variations in population response patterns can often be explained by just a few independent latent variables [21–25]. Therefore, networks with unstructured random connectivity are not able to capture the shared variability in neural population responses.

A main determinant of the connection probability between a pair of neurons in cortex is the physical distance between them [26–30]. Nearby neurons are more likely to be connected, whereas neurons that are far apart are less likely to be connected. Recently, several studies of spatially distributed neuronal networks have suggested that spatiotemporal patterns of neural activity can explain many features of variability in neural population responses [21, 31–33]. For example, our past work has shown that spiking neuron networks with irregular wave dynamics generate on average positive correlations and low-dimensional population-wide shared variability, consistent with cortical recordings [21].

Here we systematically analyze the dynamical regimes of spatially distributed firing rate networks. We find a parameter region where networks exhibit irregular chaotic dynamics. The chaotic solutions have several features of response variability that are consistent with experimental findings in cortex, such as broadband frequency power in single neuron responses, distance-dependent correlations and low-dimensionality of population responses. Interestingly, chaos occurs in networks where the excitatory and inhibitory neurons have similar projection widths, an anatomical feature found in the cortex [27, 29, 30]. Further, we find that correlated noisy inputs induce chaos, which can explain the prevalence of large-scale shared variability observed in cortex. Our work identifies a new dynamical regime of spatiotemporal chaos in neuronal networks that can account for rich response patterns in neural population activity.

Results

We study a spatially distributed network model that describes the firing rate dynamics of the excitatory (r_e) and inhibitory (r_i) neurons (Eqs 1 and 2). Neurons are organized on a two-dimensional sheet $(x \in [0, 1] \times [0, 1])$ with periodic boundary conditions (Fig 1A). The equations that describe the dynamics of the firing rates are

$$\tau_e \frac{\partial r_e(x,t)}{\partial t} = -r_e + \phi(W_{ee} g(x,\sigma_e) * r_e + W_{ei} g(x,\sigma_i) * r_i + \mu_e), \tag{1}$$

$$\tau_i \frac{\partial r_i(x,t)}{\partial t} = -r_i + \phi(W_{ie}g(x,\sigma_e) * r_e + W_{ii}g(x,\sigma_i) * r_i + \mu_i), \qquad (2)$$

where $\tau_e(\tau_i)$ is the time constant of the excitatory (inhibitory) population, * denotes convolution in space, and $\phi(x) = \max(x, 0)^2$ is the input-output transfer function of each neuron. The connection strength from a neuron in population β to a neuron in population α decays with distance as a Gaussian function, $g(x, \sigma_\beta)$, with projection width $\sigma_\beta(\alpha, \beta = e, i)$. The average connection strength from population β to population α is $W_{\alpha\beta}$. The external input to each population is a static and spatially homogeneous current, $\mu_\alpha(\alpha = e, i)$.

The spatial networks generate rich spatiotemporal patterns. In particular, we find that the network exhibits irregular patterns in both space and time for certain parameters (Fig 1B and 1C). These networks show spatially localized and transient activity patterns that sometimes propagate across the network (Fig 1B). Individual neurons show epochs of brief firing with varying magnitudes and time intervals in between (Fig 1C). This type of network dynamics result in large variability that is shared among neurons in the network. In order to better understand the behavior of the model and the mechanism for generating irregular firing patterns, we systematically analyze the different dynamical regimes of the spatially distributed networks. We focus our analysis on varying the temporal (τ_i) and spatial (σ_i) scales of the inhibitory neurons, while fixing those of the excitatory neurons ($\tau_e = 5$ ms and $\sigma_e = 0.1$).

A reduced two-unit model with no spatial coupling

We first consider networks with no spatial coupling, meaning that the spatial coupling function, *g*, is constant over distance. In this case, the network is reduced to a two-unit system,

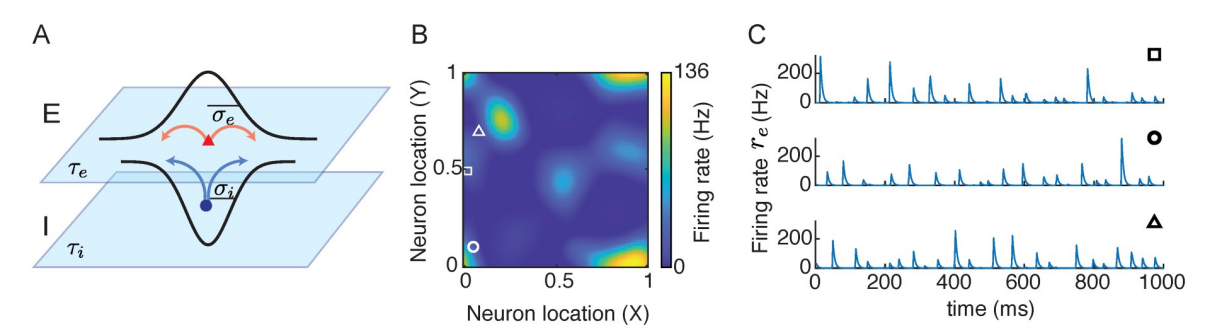


Fig 1. Irregular spatiotemporal dynamics in spatially distributed networks. A. Model schematic of recurrently coupled excitatory (E) and inhibitory (I) neurons. Neurons from each population are equally spaced on a two dimensional sheet, $[0, 1] \times [0, 1]$, with distance-dependent connectivity weights. **B.** A snapshot of the firing rates of excitatory neurons. **C.** Three examples of the time courses of firing rates of neurons at different locations. The square, circle and triangle in panel **B** denote the spatial location of each neuron.

https://doi.org/10.1371/journal.pcbi.1010843.g001

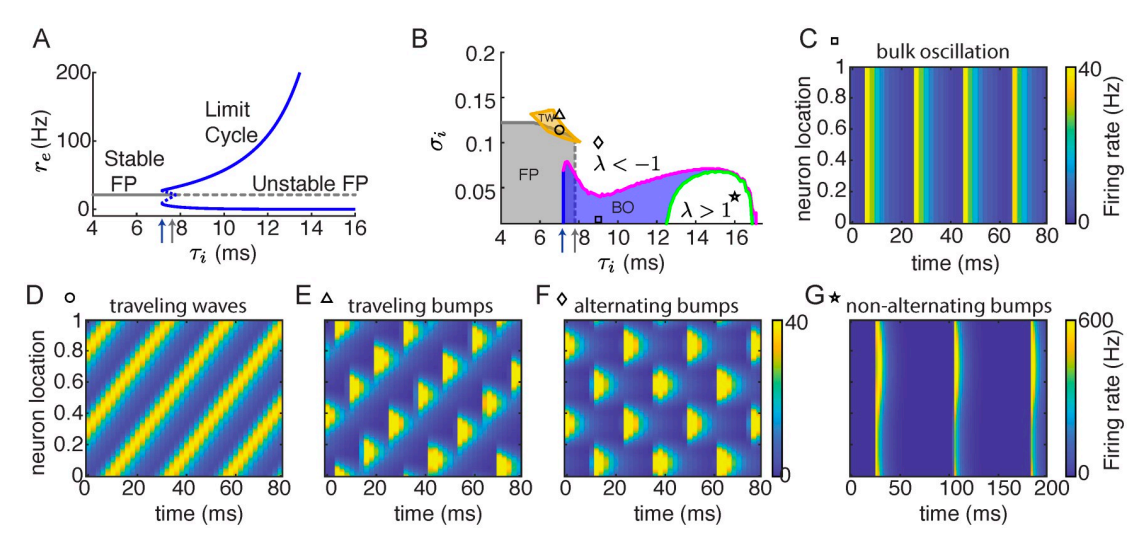


Fig 2. Dynamical regimes of networks with one-dimensional spatial coupling. A. Bifurcation diagram of the reduced two-unit model (Eqs 3 and 4) as τ_i varies. Gray line, fixed point; blue curves, the maximal and minimal firing rates of a limit cycle; solid, stable; dashed, unstable. The blue arrow indicates the lowest τ_i with a limit cycle solution. The gray arrow indicates the Hopf bifurcation (the largest τ_i with a stable fixed point solution). **B.** Phase diagram of networks with one dimensional spatial coupling. Gray, stable fixed point; blue, stable bulk oscillation; orange, stable traveling waves. The fixed point solution loses stability at either the zero wave number (gray dashed line) or a nonzero wave number (gray solid line). The bulk oscillation loses stability with either an eigenvalue becoming larger than 1 (green curve) or an eigenvalue becoming less than -1 (magenta curve). Blue and gray arrows point to the same values of τ_i as in **A.** C-G Examples of the firing rate dynamics of the excitatory neurons in networks with different τ_i and σ_i (the square, circle, triangle, diamond and star symbols indicate the parameters in panel **B**). **C**, Bulk oscillation; **D**, traveling waves; **E**, traveling bumps; **F**, alternating bumps; **G**, non-alternating bumps. The temporal and spatial scales of the excitatory neurons are $\tau_e = 5$ ms and $\sigma_e = 0.1$, respectively.

where the firing rate, $r_{\alpha}(x, t) = r_{\alpha}(t)$, $\alpha = e$, i, is independent of the neural location x.

$$\tau_e \frac{\mathrm{d}r_e}{\mathrm{d}t} = -r_e + \phi(W_{ee}r_e + W_{ei}r_i + \mu_e), \tag{3}$$

$$\tau_i \frac{\mathrm{d}r_i}{\mathrm{d}t} = -r_i + \phi(W_{ie}r_e + W_{ii}r_i + \mu_i). \tag{4}$$

Note that a solution to the two-unit system corresponds to a spatially uniform solution to the spatially distributed networks (Eqs 1 and 2).

The reduced network (Eqs 3 and 4) has a stable fixed point solution for a small τ_i (Fig 2A, gray solid line). As τ_i increases, the fixed point solution becomes unstable through a Hopf bifurcation ($\tau_i = \tau_{\text{HB}}$, Fig 2A, gray arrow), and the system admits a stable periodic solution (limit cycle; Fig 2A, blue solid curve). Over the interval of $\tau_i \in [7.16, 7.78]$ ms both the fixed point and the limit cycle solutions are stable (between the blue and gray arrows in Fig 2A). We next analyze the stability of the fixed point and the limit cycle solutions in the spatially distributed networks (Eqs 1 and 2).

Pattern formation in one-dimensional networks

In this section we analyze the stability of spatially uniform solutions and how a loss of stability leads to periodic spatiotemporal patterns. We first consider networks with one-dimensional spatial coupling, where neurons are distributed over a line interval, [0, 1], with periodic boundary conditions (namely, a ring). The stability analysis below is also applicable to two-dimensional networks.

We first analyze the stability of the fixed point solution in spatially distributed networks, which is a static and spatially uniform solution. We linearize around the fixed point in the spatial frequency domain using Fourier transform and obtain eigenvalues for each wave number (spatial frequency) (see Methods; [34, 35]). The fixed point solution is stable when all eigenvalues are negative (stable region is shown in gray in Fig 2B). When $\sigma_i < \sigma_e$, the network loses stability at zero wave number as τ_i increases, which is the same condition as the Hopf bifurcation in the two-unit model (Fig 2B, gray arrow, gray dashed line). For small σ_i and $\tau_i > \tau_{HB}$, the network exhibits spatially uniform and temporally periodic solutions (bulk oscillation; Fig 2C), which corresponds to the limit cycle solution in the two-unit model (Eqs 3 and 4). When $\sigma_i > \sigma_e$, the network loses stability at a nonzero wave number (Fig 2B, gray solid line), suggesting pattern formation of spatially and/or temporally periodic solutions.

Around the boundary where the fixed point solution loses stability at a nonzero wave number, we find traveling wave solutions (Fig 2B orange region, Fig 2D). Using a continuation numerical method [36], we show that stable traveling wave solutions exist in a small parameter region (Fig 2B, orange) that partially overlaps with the region of stable fixed point. Closely beyond this region with a larger σ_i , the traveling waves lose stability and the networks generate traveling bump solutions (Fig 2E).

We next compute the stability of the bulk oscillation solution. Similar to the stability analysis of the fixed point solution, we linearize around the bulk oscillation solution and perturb the system at different wave number (see Methods). The dynamics of the perturbation then follow a linear system of differential equations with periodic coefficients (Eq 8). The stability of the bulk oscillation solution depends on the eigenvalues (λ) of the monodromy matrix, M, of the linear system, which describes the change of the perturbation after one period of the bulk oscillation solution (Eq 9; [37, 38]). The bulk solution is unstable if there is an eigenvalue of M(k)with magnitude larger than 1 for any wave number k. We find that with small σ_i and an intermediate range of τ_i , the bulk oscillation is stable (Fig 2B, blue region; Fig 2C). As σ_i increases, the bulk oscillation loses stability with a real eigenvalue less than -1 for perturbations at a nonzero wave number, indicating a period-doubling bifurcation (Fig 2B, magenta curve). In the parameter region beyond this stability boundary, the network activity shows spatial patterns that alternate over time (Fig 2F). As τ_i increases, the bulk oscillation loses stability with a real eigenvalue larger than 1 (Fig 2B, green curve). In the region under this stability boundary (Fig 2B, green curve), the network activity exhibits spatial patterns that repeats at each cycle (Fig 2G).

Chaotic dynamics in two dimensional networks

We next analyze the full networks with two dimensional spatial coupling (Fig 1A). The stability analysis of the fixed point and the bulk oscillation that we outlined above for the one-dimensional networks is also applicable to networks of higher dimensions. The two-dimensional networks have almost identical stability boundaries for the fixed point and the bulk oscillation solutions as those in the one-dimensional networks (Fig 2B and S1 Fig). In the region above the period-doubling bifurcation curve of the bulk oscillation solution (Fig 2B, region with $\lambda < -1$), the two-dimensional networks have solutions similar to those in the one-dimensional networks, such as traveling waves (Fig 3A) and alternating bumps solutions (Fig 3B). In addition, we find other spatiotemporal patterns in the two-dimensional networks, such as spatially periodic stripe patterns that alternate in phase over time (Fig 3C).

In particular, we find network solutions that are irregular in both space and time (Figs <u>3D</u>, <u>1B and 1C</u>). In these networks, neurons exhibit random like activity with large variability even though the network is deterministic. We verify that such irregular solutions are chaotic,

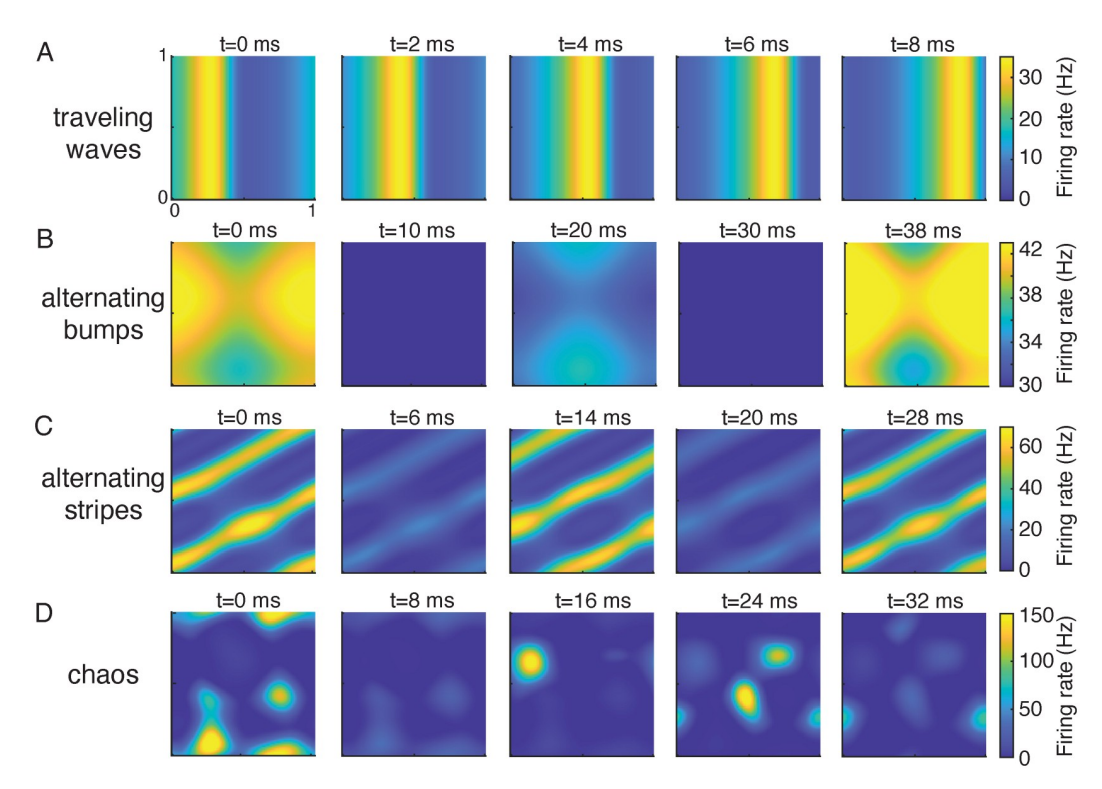


Fig 3. Examples of solutions in networks with two-dimensional spatial coupling. A-D, Snapshots of the firing rates of the excitatory population at five time frames. **A**, traveling waves solution ($\tau_i = 8$, $\sigma_i = 0.1$). **B**, alternating bumps solution ($\tau_i = 9$, $\sigma_i = 0.06$). **C**, alternating stripes solution ($\tau_i = 9$, $\sigma_i = 0.1$). **D**, chaotic solution ($\tau_i = 12.8$, $\sigma_i = 0.096$). The axes are the neuron location on the two-dimensional neuronal sheet.

meaning that a small perturbation leads to rapid divergence in network activity, by computing the maximal Lyapunov exponent (MLE) numerically (see Methods; [39]). The MLE measures the rate of separation between a perturbed trajectory and the original trajectory. The distance between the perturbed and original trajectories grows as $e^{-\lambda_{\text{MLE}}t}|dz_0|$ where $|dz_0|$ is the size of the initial perturbation. A positive MLE means that the solution is chaotic, a negative MLE indicates a stable fixed point, and MLE = 0 indicates that the solution is periodic or quasi-periodic. We compute the MLE of network solutions over the parameter space of σ_i and τ_i . We find chaotic solutions in a parameter region where the spatial scales of the excitatory and inhibitory projections are similar ($\sigma_i \approx \sigma_e = 0.1$) and the time constant of the inhibitory neurons is large ($\tau_i > \tau_e = 5$ ms) (Fig 4A, yellow). Interestingly, anatomical measurements from sensory cortices find that excitatory and inhibitory neurons project on similar spatial scales [29, 30, 40]. In addition, the decay kinetics of inhibitory synaptic currents are also slower than the excitatory synaptic currents in physiology [28, 41, 42]. These results suggest that the network parameter region of chaotic dynamics is consistent with the anatomy and physiology of the cortex. In contrast, networks with one-dimensional spatial coupling have a restricted parameter region of chaos, suggesting that the two-dimensional spatial structure is important for generating chaos (S2 Fig).

Population statistics of the chaotic solutions

Networks with chaotic dynamics intrinsically generate large variability in population activity. We next measure statistics of the population activity of networks in the chaotic regime and

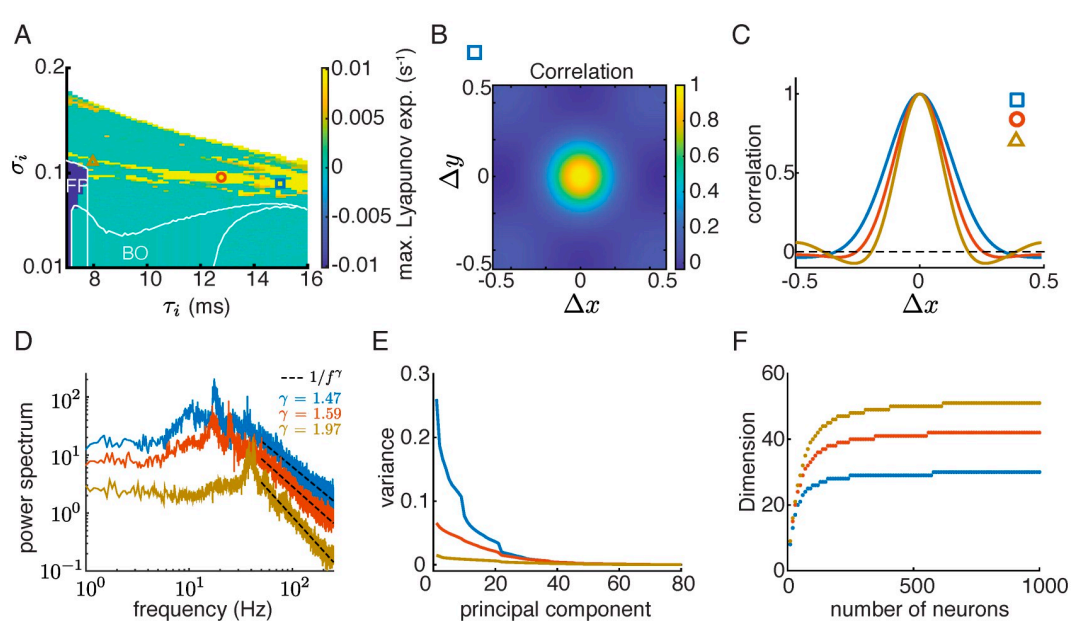


Fig 4. Population statistics of the chaotic solutions. A. The maximal Lyapunov exponent (MLE) as a function of the projection width (σ_i) and the time constant (τ_i) of the inhibitory population for the two-dimensional networks. The white curves are the stability borders of the parameter regions of stable fixed point (FP) and bulk oscillation (BO) solutions (same regions as in Fig 2B and S1 Fig). The color axis is limited at ± 0.01 to better visualize the region of positive MLE's (i.e. chaos region). **B.** The correlation between neuron activity as a function of distance in x and y directions (Eq 11) in a network labeled as a blue square in panel A. **C.** The correlation function along the x direction for three networks in the chaotic regime ($\Delta y = 0$). The network parameters are denoted in panel A with corresponding symbols. **D.** Population averaged power spectrum of single-neuron rate activity represented in log-log scale (Eq 12). Dashed lines represent 1/f' scaling. **E.** The variance of the dominant principal components of population rate activity of 1000 randomly sampled neurons from the networks, averaged over 100 samples. **F.** The dimension of population activity saturates as the number of sampled neurons increases. The dimension is defined as the number of dominant principal components that account for 95% of the total variance. Snapshots of network activity from the three networks in C-F are shown in S3 Fig.

compare with cortical recordings. First, we compute the spatial correlations of population activity along x and y directions (Fig 4B and 4C, see Methods). The spatial correlations of the chaotic dynamics are roughly isotropic, and decrease with the distance between neurons (Fig 4B). A vanishing correlation at large distance and a positive Lyapunov exponent are the defining signatures of spatiotemporal chaos [43]. The decrease of correlation with cortical distance has been widely reported in population recordings across the cortex [19, 44–48]. Further, we found that the spatial decay rate of correlation depends on network parameters. Networks with larger τ_i have a broader range of correlation which remains positive over long distance (Fig 4C).

Second, we measure the power spectrum of the temporal variability of each neuron unit. We find that neurons in chaotic networks have broadband frequency power with peaks at around 20–40 Hz (Fig 4D). Beyond about 50 Hz, the power decays with frequency following a power law scaling (1/f') with exponent (γ) between 1.5 and 2 (Fig 4D dashed). This means that the neurons' rate activities are not periodic as those in regular solutions, but exhibit considerable variability over a broad frequency range. This type of broadband frequency power has also been found in many neural recordings [49–51]. A power-law relationships is often regarded as a sign for self-organized critical states in network dynamics [52, 53]. However, power-law scaling can also arise from stochastic dynamics without being at critical states [54, 55]. The chaos in our networks does not result from a critical transition, which would imply

scale-free temporal and spatial correlations. Instead, the chaotic dynamics in our networks have a characteristic temporal frequency and spatial scale of correlations.

Lastly, we examine the dimensionality of the chaotic solutions. We perform principal component analysis of the rate activity of 1000 randomly sampled neurons from the networks. The variance of each principal component is the eigenvalue of the covariance matrix of population rate over time, sorted from large to small. We find that the variability of the chaotic population rate concentrates in the first few tens of principal components (Fig 4E). We define the dimension of the population activity as the number of principal components that explains 95% of the variance. The dimension of chaotic solutions increases with the number of sampled neurons and saturates below 50 (Fig 4F), which is much lower than the number of neurons in the network ($N = 10^4$). The low dimensional structure is a defining feature of cortical neural variability that has been recently demonstrated in multiple population recordings [20–24]. In contrast, the chaotic rate dynamics in disordered random networks have dimensions that increase linearly with network size [56].

Transition to chaos through quasi-periodicity and intermittency

To further investigate how network dynamics transition from a regular solution to chaos, we vary the inhibitory projection width (σ_i) with fixed inhibitory time constant τ_i . We find that the network transitions into chaos through quasi-periodicity and intermittency as σ_i increases (Fig 5). For each σ_i , we show an example trial of rate dynamics from a vertical slice of the excitatory population (Fig 5 column 1), a phase plot of two excitatory neurons from different locations (Fig 5 column 2), the temporal power spectrum of single-neuron rate activity (Fig 5 column 3) and spatial correlations (Fig 5 column 4).

Beyond the period-doubling bifurcation of the bulk oscillation solution (Fig 2B and S1 Fig, magenta curves), the network has alternating bump solutions (Figs 5A and 3B). We can see that the solution is periodic both from the spatiotemporal activity from one slice of the network (Fig 5A1) and the phase plot of firing rates of two excitatory neurons (Fig 5A2). For this solution, the temporal power spectrum has sharp peaks at harmonic frequencies and the spatial correlation is large across all distances. As σ_i increases, the alternating bump solution loses stability and leads to quasi-periodic solutions with alternating stripe patterns (Fig 5B, similar to the solution in Fig 3C). The temporal power spectrum shows sharp frequency peaks (Fig 5B3) and the spatial correlation shows a diagonal stripe pattern (Fig 5B4). As σ_i further increases, the network shows intermittent behavior with alternating stripes interspersed with irregular activity (Fig 5C1, irregular activity around 500 ms). The MLE is positive for this network, indicating a chaotic solution. The spatial correlation peaks at the center and the opposite corners because the alternating stripes switch orientations from time to time (Fig 5C4). After a narrow parameter range of intermittent activity, the chaotic solution becomes more irregular with Gaussian-like spatial correlations that decay to zero at large distance (Fig 5D4). The temporal power spectrum contains a broad range of frequency power (Fig 5D3). Lastly, for larger σ_n chaotic solutions disappear and the network shows complex quasi-periodic activity (Fig 5E).

Correlated input noise expands the chaotic regime

We have, thus far, analyzed the behavior of fully deterministic networks. We now consider how input noise changes network dynamics. The input to neuron k from population α is

$$I_k^{\alpha} = \mu_{\alpha} + \sigma_n (\sqrt{1 - c} \cdot \eta_k^{\alpha} + \sqrt{c} \cdot \eta_c^{\alpha}), \tag{5}$$

where σ_n is the standard deviation and $c \in [0, 1]$ is the correlation coefficient of the input

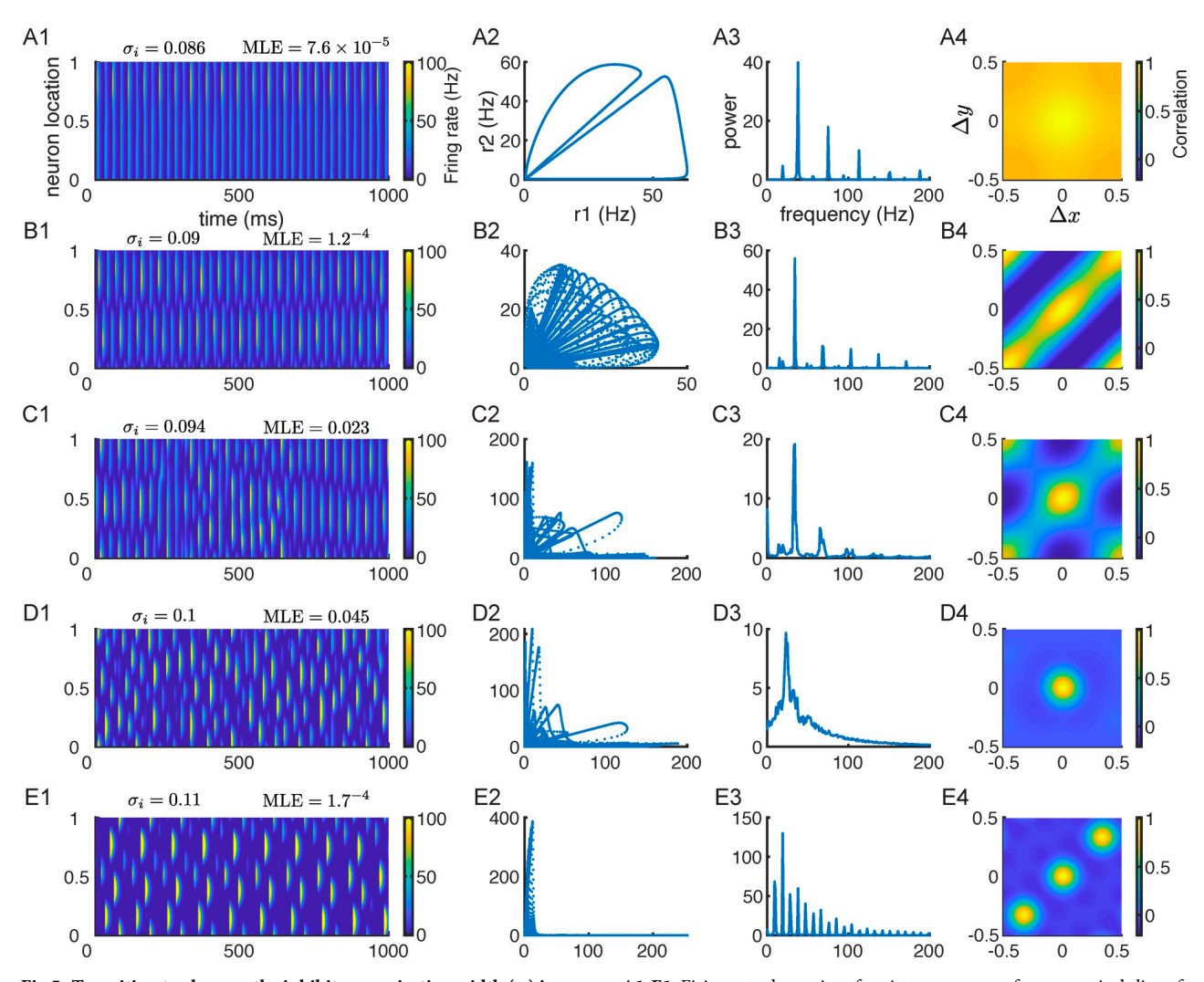


Fig 5. Transition to chaos as the inhibitory projection width (σ_i) increases. A1-E1. Firing rate dynamics of excitatory neurons from a vertical slice of the network. The MLE of the solution is shown on top. A2-E2. Phase plots of firing rates of two excitatory neurons from different locations. A3-E3. Population averaged power spectrum of single-neuron rate activity (Eq 12). A4-E4. The correlation between neuron activity as a function of distance in x and y directions (Eq 11). The inhibitory time constant is fixed as $\tau_i = 11$ ms.

noise. The input noise to each neuron consists of two components: 1) an independent noise component, η_k^{α} , which is private to each neuron k, and 2) a correlated noise component, η_c^{α} , which is common for all neurons in population $\alpha \in \{e, i\}$ (Fig 6A; [57, 58]). Both noise components are modeled as Ornstein–Uhlenbeck processes with time constant $\tau_n = 5$ ms (see Methods, Eq 13). The amplitude of the independent noise component is $\sigma_n \sqrt{1-c}$ and the amplitude of the correlated component is $\sigma_n \sqrt{c}$.

When the input noise is weak (small σ_n), the regular solutions can roughly maintain their spatiotemporal patterns (Fig 6B). However, when the input noise is strong (large σ_n), the patterns might be distorted or completely destroyed. For example, a network that produces traveling waves without input noise (Fig 3A) can still generate a noisy traveling wave pattern with weak noise (Fig 6B), but exhibits irregular patterns when input noise is strong (Fig 6C).

The irregular spatiotemporal patterns in networks with strong noise are similar to the chaotic solutions in deterministic networks (Fig 3A). We next compute the MLE of networks with

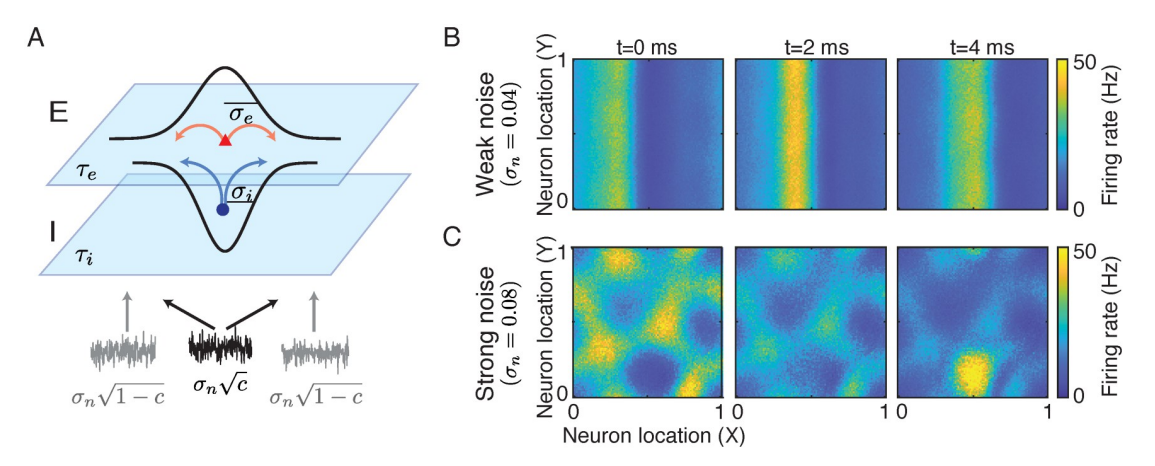


Fig 6. Two-dimensional networks with input noise. A. The input noise to each neuron consists of a correlated noise component (black) that is common for all neurons from the same population, and an independent noise component that is private to each neuron (gray). **B-C.** Snapshots of the firing rates of the excitatory population at three time frames for a network that generates traveling waves when there is no input noise ($\tau_i = 8$, $\sigma_i = 0.1$, same parameters as in Fig 3A). The correlation of the input noise is c = 0.5, and the amplitude is $\sigma_n = 0.04$ (**B**) and $\sigma_n = 0.08$ (**C**).

frozen input noise in the parameter space of σ_i and τ_i (see Methods). We find that input noise can induce chaos in the spatially distributed networks. With correlated input noise, the parameter region of chaotic solutions expands as the amplitude of noise increases (compare yellow regions in Figs 4A and 7A and 7B). This suggests that a network receiving correlated input, for example from an upstream area, is more likely to generate chaotic dynamics than a network receiving static input without noise, which can potentially explain the prevalence of correlated activity across cortex.

In addition to inducing chaos, we find that noise can also synchronize bulk oscillations, reflected as negative MLE's in the previously identified regime of bulk oscillations (light blue area in Fig 7A and 7B). A negative MLE of a noise driven system means that networks starting at different initial conditions would converge to the same network dynamical trajectory that depends only on the noise realization [59, 60].

Further, we investigate the impacts of the amplitude (σ_n) and the correlation (c) of input noise on network dynamics. We compute the MLE of four examples of periodic solutions with varying σ_n and c (Fig 7C–7F). When there is no input noise $(\sigma_n = 0)$, the MLE's of these networks are zero, since they produce temporally periodic patterns. When driven by independent noise (c = 0), the MLE's remain close to zero, which suggests that the periodic solutions are insensitive to independent noise. As σ_n and c increase, the MLE's generally increase and become positive, indicating a transition to chaos (Fig 7C–7E). The bulk oscillation solution becomes synchronized with negative MLE for intermediate values of σ_n and c before transitioning to chaos (Fig 7F).

We next measure how MLE depends on the amplitude of the correlated noise component, $\sigma_n \sqrt{c}$ (Fig 6A). When plotting as a function of $\sigma_n \sqrt{c}$, the MLE's for varying σ_n and c collapse to a single function curve (Fig 7G–7J). This suggests that the MLE of the noise driven system mainly depends on the amplitude of the correlated noise component. The transition to chaos can be sharp, as in the cases of traveling waves and alternating stripes (Fig 7G and 7I), or gradual, as in the cases of alternating bumps and bulk oscillation (Fig 7D and 7F). Therefore, we identify that it is the correlated noise component that is responsible for inducing chaos and synchronizing bulk oscillations in the two-dimensional networks. In contrast, the network dynamical patterns are insensitive to independent noise.

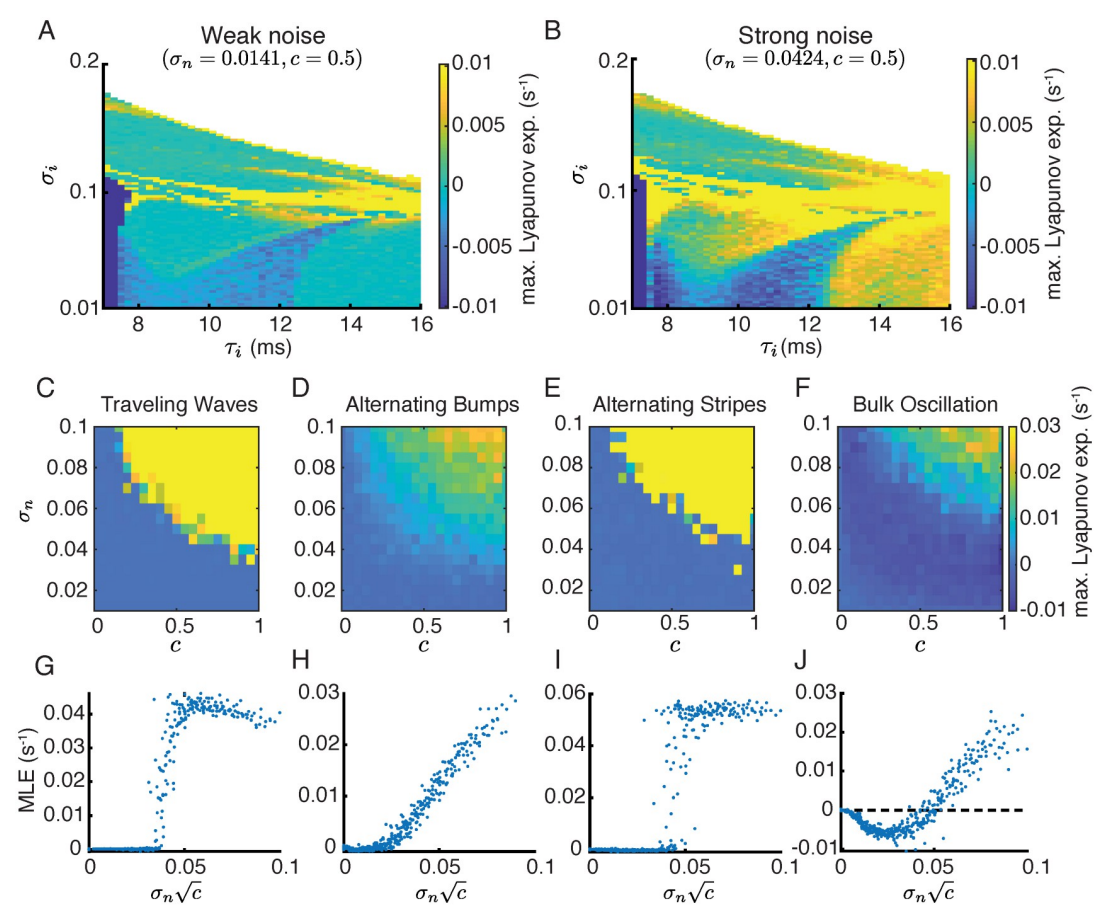


Fig 7. The maximal Lyapunov exponent (MLE) for the two-dimensional networks with input noise. A-B. The MLE map with weak (**A**, $\sigma_n = 0.0141$) and strong (**B**, $\sigma_n = 0.0424$) noise. The correlation of the input noise is c = 0.5. **C-F**. MLE as a function of the amplitude (σ_n) and the correlation (c) of input noise, for four example networks that generate traveling waves (C; $\tau_i = 8$, $\sigma_i = 0.1$, same as Fig 3A), or alternating bumps (D; $\tau_i = 9$, $\sigma_i = 0.06$, same as Fig 3B), or alternating stripes (E; $\tau_i = 9$, $\sigma_i = 0.1$, same as Fig 3C) or bulk oscillation (F; $\tau_i = 8$, $\sigma_i = 0.03$) without noise. **G-J**. Same as panels C-F with MLE as a function of the amplitude of the correlated noise component, $\sigma_n \sqrt{c}$.

Discussion

Variability in neural responses is prevalent in cortex. The structure of the variability shared among a neuron population has important consequences on the information processing of the network [61]. However, the circuit mechanism underlying neural variability remains unclear. In this work, we discover a new dynamical regime in spatially distributed neuronal networks where spatiotemporal chaos produce large magnitude of shared variability in population activity. The statistical properties of the spatiotemporal chaos are consistent with population recordings from cortex, such as the broadband frequency power in single neuron responses, distance-dependent correlations and the low dimensionality of population responses.

Our model incorporates a few generic biological features of cortical circuits. First, the synaptic connections between neurons are spatially organized, meaning that the connection probability between a pair of neurons strongly depends on the physical distance between them [26, 28–30, 40, 62]. Importantly, it has been found that the excitatory and inhibitory projections have a similar spatial footprints [29, 30, 40], which is also the network condition where we find chaotic dynamics. Second, the decay kinetics of inhibitory synaptic currents are much slower

than the excitatory synaptic currents in physiology [28, 41, 42]. We find that slow inhibition is important to generate complex spatiotemporal dynamics. Lastly, we use a power-law transfer function of rate response, which has been found to well describe neuron responses measured in cat visual cortex [63]. Power-law transfer functions have also shown to be critical to explaining various features of neural responses from the visual cortex, such as contrast invariance of tuning, sublinear response summation and surround suppression [64–66]. We show that neural networks with these biological features generate complex spatiotemporal dynamics whose population statistics match those from cortical recordings during the awake state.

Rate chaos in neuronal networks has been widely studied using random recurrent networks, where the connection weights from each neuron follow a Gaussian distribution with zero mean [9]. The network solution transitions from a stable fixed point to chaos when the variance of connection weights exceeds a critical value. Similar transition to chaos is also observed in networks with separate excitatory and inhibitory populations [67] and in spiking neuron networks [68]. In contrast, in spatially distributed networks, chaos appears after several solutions of different spatiotemporal patterns lose stability. As σ_i increases, the bulk oscillation solutions transition to alternating bump solutions, which transition to alternating stripes or traveling waves, and then to chaos (Fig.5). Further theoretical analysis is needed to elucidate the transition to chaos in spatial networks.

The spatiotemporal chaos in our networks has several distinct features from the chaotic solutions in random neuronal networks [9, 11, 69]. First, in networks of unstructured random connectivity, the correlations among neurons vanish as network size becomes large (scales as $1/\sqrt{N}$ with N being the network size) [11, 70]. Hence, those networks do not generate correlated population patterns, while the chaos in spatial networks produce distance-dependent correlations. Second, the dimensionality of population activity in random networks has been found to be high and increases linearly with network size [56]. This is in contrast with the low dimensional structure of the spatiotemporal chaos found in spatial networks (Fig 4F) and population activity found in experimental data [20–24]. Lastly, previous work showed that time varying inputs, such as independent white noise and oscillatory inputs, suppress chaos [11, 56, 69, 71, 72], while we found that the chaotic solutions in spatial networks are insensitive to independent noise and that chaos can be induced by correlated noise (Fig 7). This provides a testable prediction that a spatially global and time-varying stimulation can desynchronize strong oscillations and increase irregularity in population activity.

Spatiotemporal chaos in distributed excitable systems has been studied in different models, such as fluid turbulence, coupled oscillators and coupled maps [43, 73]. Most of the models are reaction-diffusion models and chaos is induced by diffusion. In contrast, our model is a system of integro-differential equations with non-local coupling. In neural network models, spatiotemporal chaos has been demonstrated in networks with local coupling [74, 75]. In [74] spatiotemporal chaos occurs in networks with a large diffusion coefficient of the inhibitory membrane potential, which models for local electrical coupling such as gap junctions. In contrast, we find chaos when the inhibitory neurons have a similar spatial scale as the excitatory neurons. The spatiotemporal chaos in their networks is caused by an interplay between Turing and Hopf instabilities of the fixed point solution, where both a nonzero and the zero wave number lose stability. This is not the case in our model, where both the fixed point and the bulk oscillation solutions are destabilized at multiple wave numbers in the parameter region of chaos (S4B and S4C Fig). Similar to our model, they also need the time constant of the inhibitory population to be large. [75] studies networks with local coupling (such as nearest neighbor coupling) among excitatory neurons and distance-dependent delays. They show that spatiotemporal chaos can appear when the network size is large. Similar to our model, they also find

spatiotemporal chaos after the bulk oscillation solution loses stability and find intermittent solutions before the appearance of spatiotemporal chaos. Delays have been shown to generate various spatiotemporal patterns [76] and may play a similar role to the inhibitory time constant (τ_i) in our model. In neither of these works are the effects of noisy inputs studied.

Several recent models have studied chaos in random neuronal networks with structured connectivity. For example, networks with a low rank connectivity component in addition to a random component can generate low dimensional coherent chaos, which can be utilized for complex computations [77, 78]. Networks with cell-type-dependent distributions of connections can produce chaos with multiple modes of autocorrelation functions of individual neurons [79]. In this work, we demonstrate that networks with two-dimensional spatial couplings and no random connectivity can also generate chaos which resides in a low-dimensional state space. How random connectivity in combination with spatially ordered connectivity affect chaos remain to be studied in future work.

Chaotic dynamics in neuronal networks offer a rich "reservoir" of population activity patterns, which can be utilized to learn a target output function or accomplish complex neural computations [12, 33, 80–82]. Near the transition of chaos, networks can generate slow dynamics which are important for temporal integration and necessary for many behavioral tasks [13, 83]. Information diffusion within a network has been found to be high in the regime of spatiotemporal chaos suggesting rapid mixing of information [75]. Here we find a new type of spatiotemporal chaos in networks where the connectivity features are consistent with cortical anatomy. It would be fruitful to explore the computational benefits of such chaos in spatially distributed networks.

Methods

Stability of fixed point solutions

Linearization around the fixed point solution (\bar{r}_e, \bar{r}_i) of Eqs 1 and 2 in Fourier space gives a Jacobian matrix at each spatial Fourier mode:

$$J(\vec{n}) = \begin{pmatrix} (-1 + L_e W_{ee} \tilde{g}(\vec{n}, \sigma_e))/\tau_e & L_e W_{ei} \tilde{g}(\vec{n}, \sigma_i)/\tau_e \\ L_i W_{ie} \tilde{g}(\vec{n}, \sigma_e)/\tau_i & (-1 + L_i W_{ii} \tilde{g}(\vec{n}, \sigma_i))/\tau_i \end{pmatrix}, \tag{6}$$

where \vec{n} is the Fourier mode, $\tilde{g}(\vec{n}, \sigma_{\alpha}) = \exp(-2||\vec{n}||^2 \pi^2 \sigma_{\alpha}^2)$ is the Fourier Gaussian kernel, and $L_{\alpha} = \phi'(u_{\alpha}^*)$ evaluated at the fixed point $u_{\alpha}^* = W_{\alpha}\bar{r}_i + W_{\alpha}\bar{r}_i + \mu_{\alpha}$, $\alpha = \{e, i\}$.

The fixed point is stable if all eigenvalues of $J(\vec{n})$ have negative real part for any \vec{n} (Fig 2B). Note that the stability only depends on the wave number $k = ||\vec{n}||$.

Stability of bulk oscillation solutions

To analyze the stability of bulk oscillation solutions, we linearize around the time dependent limit cycle solution, $(\bar{r}_e(t), \bar{r}_i(t))$, and obtain the Jacobian matrix at each Fourier mode, which is also periodic in time [37, 38]:

$$J(\vec{n};t) = \begin{pmatrix} (-1 + L_e(t)W_{ee}\tilde{g}(\vec{n},\sigma_e))/\tau_e & L_e(t)W_{ei}\tilde{g}(\vec{n},\sigma_i)/\tau_e \\ L_i(t)W_{ie}\tilde{g}(\vec{n},\sigma_e)/\tau_i & (-1 + L_i(t)W_{ii}\tilde{g}(\vec{n},\sigma_i))/\tau_i \end{pmatrix}, \tag{7}$$

where $L_{\alpha}(t) = \phi'(u_{\alpha}^*(t))$ evaluated along the limit cycle solution $u_{\alpha}^* = W_{\alpha e} \bar{r}_e(t) + w_{\alpha i} \bar{r}_i(t) + \mu_{\alpha}$, $\alpha = \{e, i\}$. The perturbation of rate, $\delta \tilde{\mathbf{r}}(\vec{n})$, at Fourier mode, \vec{n} , follows a linear system with

periodic coefficients:

$$\frac{d\delta\tilde{\mathbf{r}}(\vec{n})}{dt} = J(\vec{n};t) \cdot \delta\tilde{\mathbf{r}}(\vec{n}). \tag{8}$$

We obtain a principal fundamental matrix solution of Eq.8 by solving $X' = J(\vec{n}; t)X$ with initial conditions X(0) = I, where I is the identity matrix. The stability of the bulk oscillation solution is then determined by the eigenvalues of the monodromy matrix,

$$M(\vec{n}) = X(\vec{n}; T), \tag{9}$$

where T is the period of the bulk oscillation solution. If any of the eigenvalues of $M(\vec{n})$ have magnitude greater than 1 at some Fourier model \vec{n} , then the bulk oscillation will lose stability with spatial mode \vec{n} . A real eigenvalue less than -1 indicates a period-doubling bifurcation, while a real eigenvalue larger than 1 suggests a pattern formation with the same period as the bulk oscillation [37].

Maximal Lyapunov exponent

The maximal Lyapunov exponent (MLE) is computed numerically using the method by [39]. We first simulate the network long enough such that the solution has converged to an attractor. We denote the solution trajectory as $\vec{R}(t) = (r_e(x, t), r_i(x, t))^T$.

We continue simulating the trajectory for n time points, $\{t_0, t_1, \ldots, t_n\}$, with step size Δt . At the initial time point, t_0 , we perturb the trajectory, $\vec{R}(t)$, by $d\vec{z}_0$, which is in a random direction and has a small magnitude $|d\vec{z}_0| = dM$. We integrate the same model system with the perturbed initial condition, $\vec{R}(t_0) + d\vec{z}_0$, by one time step, Δt , and obtain the perturbed trajectory, $\vec{R}_p(t_1)$. The separation between the two trajectories is $D\vec{z}_1 = \vec{R}_p(t_1) - \vec{R}(t_1)$. Then we choose the perturbation at the next time step as $d\vec{z}_1 = \frac{D\vec{z}_1}{|D\vec{z}_1|}dM$. In this way, the perturbation in each time point has a magnitude of dM, and is in the same direction as the separation between the original and the perturbed trajectories at the previous time step. We then integrate the same model system with the perturbed initial condition, $\vec{R}(t_1) + d\vec{z}_1$, by one time step and obtain $\vec{R}_p(t_2)$. We repeat this procedural n steps and obtain a sequence of trajectory separations, $(D\vec{z}_i)_{i=0}^n$. Lastly, the Maximal Lyapunov exponent is computed as

$$MLE = \frac{1}{n\Delta t} \sum_{i=1}^{n} \log(|D\vec{z}_i|/dM), \tag{10}$$

where $n = 10^6$ and $\Delta t = 0.01s$. The MLE converges at large n (S5 Fig).

Spatial correlation

The spatial correlations in Fig 4B and 4C are defined as the Pearson correlation coefficient of r_{∞} for each neural distance $(\Delta x, \Delta y)$:

$$C(\Delta x, \Delta y) = \frac{\langle (r_e(x + \Delta x, y + \Delta y, t) - \langle r_e(x + \Delta x, y + \Delta y, t) \rangle_t) (r_e(x, y, t) - \langle r_e(x, y, t) \rangle_t) \rangle_{x,y,t}}{\operatorname{Var}(r_e(x, y, t))}, (11)$$

where $\langle \cdot \rangle_t$ is average over time and $\langle \cdot \rangle_{x,v,t}$ denotes average over time and space.

Power spectrum

The power spectrum in Fig 4D is defined as:

$$S = \langle |F(r_e - \langle r_e \rangle_t)|^2 \rangle_{x,y}, \qquad (12)$$

where the function *F* is the Fourier transform in time.

Input noise

The input noise terms η_k^{α} and η_c^{α} ($\alpha \in \{e, i\}$) in Eq.5 are modeled as independent Ornstein–Uhlenbeck processes:

$$\tau_n d\eta = -\eta dt + dW,\tag{13}$$

where *W* is a Wiener process, and the noise time constant is $\tau_n = 5$ ms.

Network parameters

Unless specified otherwise, the network parameters are $W_{ee} = 80$, $W_{ei} = -160$, $W_{ie} = 80$, $W_{ii} = -150$, $\tau_e = 5$ ms, $\sigma_e = 0.1$, $\mu_e = 0.48$ and $\mu_i = 0.32$. τ_i and σ_i vary in each figure and are specified in figure axes and captions. The number of neurons in the two dimensional network are $N = 100 \times 100$ for each of the excitatory and inhibitory populations. In the one dimensional network N = 100 for each of the populations.

Supporting information

S1 Fig. Related to Fig 3. Phase diagram of networks with two dimensional spatial coupling. Same format as Fig 2B in the main text. The letters mark the locations of the parameters used in Fig 3A–3D. (TIFF)

S2 Fig. Related to Fig 4. The maximal Lyapunov exponents of networks with one dimensional spatial coupling. Same format as Fig 4A. The maximal Lyapunov exponent as a function of the projection width (σ_i) and the time constant (τ_i) of the inhibitory neurons. The white curves are the stability borders of the parameter regions of stable fixed point (FP) and bulk oscillation (BO) solutions (same regions as in Fig 2B). (TIFF)

S3 Fig. Related to Fig 4. Snapshots of the firing rates of the excitatory population at five time frames from the three chaotic solutions in Fig 4. There is no qualitative difference in the activity.

(TIFF)

S4 Fig. Related to Fig 4. A. The maximal Lyapunov exponent (MLE) as a function of the projection width (σ_i) and the time constant (τ_i) of the inhibitory population for the two-dimensional networks. Same as Fig 4A in the main text. **B.** The number of unstable wave numbers from the stability analysis of the bulk oscillation solution. **C,** The number of unstable wave numbers from the stability analysis of the fixed point solution. Orange dots in panels B and C denote the chaos region shown in panel A with MLE>0.005. **A-C.** Same network parameter as in Fig 4 of the main text. **D-F.** Same parameters as A-C except that W_{ie} is changed from 80 to 100.

(TIFF)

S5 Fig. Related to Methods: Maximal Lyapunov exponent. Convergence of the maximal Lyapunov exponent as a function of the number of perturbations n (Eq 10). Each curve is the MLE for one solution. There are 10 chaotic solutions (MLE>0.005) and 5 periodic solutions (MLE<0.002). (TIFF)

Acknowledgments

We thank Daniele Avitabile for his code and discussion regarding computing the stability of the traveling wave regime (Fig 2B). We thank Jonathan Kadmon for the consultation regarding the MLE computation.

Author Contributions

Conceptualization: Noga Mosheiff, Bard Ermentrout, Chengcheng Huang. **Formal analysis:** Noga Mosheiff, Bard Ermentrout, Chengcheng Huang.

Funding acquisition: Chengcheng Huang.

Investigation: Noga Mosheiff, Bard Ermentrout, Chengcheng Huang.Methodology: Noga Mosheiff, Bard Ermentrout, Chengcheng Huang.

Supervision: Chengcheng Huang.

Validation: Noga Mosheiff. Visualization: Noga Mosheiff.

Writing - original draft: Noga Mosheiff.

Writing - review & editing: Bard Ermentrout, Chengcheng Huang.

References

- Shadlen MN, Newsome WT. The variable discharge of cortical neurons: implications for connectivity, computation, and information coding. The Journal of neuroscience. 1998; 18(10):3870–3896. https://doi.org/10.1523/JNEUROSCI.18-10-03870.1998
- Kara P, Reinagel P, Reid RC. Low response variability in simultaneously recorded retinal, thalamic, and cortical neurons. Neuron. 2000; 27(3):635–646. https://doi.org/10.1016/S0896-6273(00)00072-6
 PMID: 11055444
- Arieli A, Sterkin A, Grinvald A, Aertsen A. Dynamics of ongoing activity: explanation of the large variability in evoked cortical responses. Science. 1996; 273(5283):1868–1871. https://doi.org/10.1126/science.273.5283.1868 PMID: 8791593
- 4. Muller L, Reynaud A, Chavane F, Destexhe A. The stimulus-evoked population response in visual cortex of awake monkey is a propagating wave. Nature communications. 2014; 5(1):1–14. https://doi.org/10.1038/ncomms4675 PMID: 24770473
- Waschke L, Tune S, Obleser J. Local cortical desynchronization and pupil-linked arousal differentially shape brain states for optimal sensory performance. Elife. 2019; 8:e51501. https://doi.org/10.7554/elife.51501 PMID: 31820732
- McGinley MJ, Vinck M, Reimer J, Batista-Brito R, Zagha E, Cadwell CR, et al. Waking state: rapid variations modulate neural and behavioral responses. Neuron. 2015; 87(6):1143–1161. https://doi.org/10.1016/j.neuron.2015.09.012 PMID: 26402600
- Doiron B, Litwin-Kumar A, Rosenbaum R, Ocker G, Josic K. The mechanics of state dependent neural correlations. Nature neuroscience. 2016; 19(3):383–393. https://doi.org/10.1038/nn.4242 PMID: 26906505
- Ni AM, Ruff DA, Alberts JJ, Symmonds J, Cohen MR. Learning and attention reveal a general relationship between population activity and behavior. Science. 2018; 359(6374):463–465. https://doi.org/10.1126/science.aao0284 PMID: 29371470

- Sompolinsky H, Crisanti A, Sommers HJ. Chaos in random neural networks. Physical Review Letters. 1988; 61(3):259. https://doi.org/10.1103/PhysRevLett.61.259 PMID: 10039285
- Van Vreeswijk C, Sompolinsky H. Chaos in neuronal networks with balanced excitatory and inhibitory activity. Science. 1996; 274(5293):1724–1726. https://doi.org/10.1126/science.274.5293.1724 PMID: 8939866
- Rajan K, Abbott L, Sompolinsky H. Stimulus-dependent suppression of chaos in recurrent neural networks. Physical Review E. 2010; 82(1):011903. https://doi.org/10.1103/PhysRevE.82.011903 PMID: 20866644
- Sussillo D, Abbott LF. Generating coherent patterns of activity from chaotic neural networks. Neuron. 2009; 63(4):544–557. https://doi.org/10.1016/j.neuron.2009.07.018 PMID: 19709635
- Toyoizumi T, Abbott L. Beyond the edge of chaos: Amplification and temporal integration by recurrent networks in the chaotic regime. Physical Review E. 2011; 84(5):051908. https://doi.org/10.1103/ PhysRevE.84.051908 PMID: 22181445
- Bertschinger N, Natschläger T. Real-time computation at the edge of chaos in recurrent neural networks. Neural computation. 2004; 16(7):1413–1436. https://doi.org/10.1162/089976604323057443
 PMID: 15165396
- Laje R, Buonomano DV. Robust timing and motor patterns by taming chaos in recurrent neural networks. Nature neuroscience. 2013; 16(7):925–933. https://doi.org/10.1038/nn.3405 PMID: 23708144
- **16.** Jaeger H, Haas H. Harnessing nonlinearity: Predicting chaotic systems and saving energy in wireless communication. science. 2004. https://doi.org/10.1126/science.1091277 PMID: 15064413
- Cohen MR, Kohn A. Measuring and interpreting neuronal correlations. Nature neuroscience. 2011; 14 (7):811–819. https://doi.org/10.1038/nn.2842 PMID: 21709677
- Schulz DP, Sahani M, Carandini M. Five key factors determining pairwise correlations in visual cortex. Journal of neurophysiology. 2015; 114(2):1022–1033. https://doi.org/10.1152/jn.00094.2015 PMID: 26019310
- Smith MA, Sommer MA. Spatial and temporal scales of neuronal correlation in visual area V4. Journal of Neuroscience. 2013; 33(12):5422–5432. https://doi.org/10.1523/JNEUROSCI.4782-12.2013 PMID: 23516307
- Lin IC, Okun M, Carandini M, Harris KD. The nature of shared cortical variability. Neuron. 2015; 87 (3):644–656. https://doi.org/10.1016/j.neuron.2015.06.035 PMID: 26212710
- Huang C, Ruff DA, Pyle R, Rosenbaum R, Cohen MR, Doiron B. Circuit Models of Low-Dimensional Shared Variability in Cortical Networks. Neuron. 2019; 101(2):337–348. https://doi.org/10.1016/j.neuron.2018.11.034 PMID: 30581012
- Williamson RC, Cowley BR, Litwin-Kumar A, Doiron B, Kohn A, Smith MA, et al. Scaling Properties of Dimensionality Reduction for Neural Populations and Network Models. PLOS Computational Biology. 2016; 12(12):e1005141. https://doi.org/10.1371/journal.pcbi.1005141 PMID: 27926936
- Ruff DA, Xue C, Kramer LE, Baqai F, Cohen MR. Low rank mechanisms underlying flexible visual representations. Proceedings of the National Academy of Sciences. 2020; 117(47):29321–29329. https://doi.org/10.1073/pnas.2005797117 PMID: 33229536
- Schölvinck ML, Saleem AB, Benucci A, Harris KD, Carandini M. Cortical state determines global variability and correlations in visual cortex. Journal of Neuroscience. 2015; 35(1):170–178. https://doi.org/10.1523/JNEUROSCI.4994-13.2015 PMID: 25568112
- Semedo JD, Zandvakili A, Machens CK, Byron MY, Kohn A. Cortical areas interact through a communication subspace. Neuron. 2019; 102(1):249–259. https://doi.org/10.1016/j.neuron.2019.01.026 PMID: 30770252
- Oswald AMM, Doiron B, Rinzel J, Reyes AD. Spatial profile and differential recruitment of GABAB modulate oscillatory activity in auditory cortex. Journal of Neuroscience. 2009; 29(33):10321–10334. https://doi.org/10.1523/JNEUROSCI.1703-09.2009 PMID: 19692606
- Mariño J, Schummers J, Lyon DC, Schwabe L, Beck O, Wiesing P, et al. Invariant computations in local cortical networks with balanced excitation and inhibition. Nature neuroscience. 2005; 8(2):194–201. https://doi.org/10.1038/nn1391 PMID: 15665876
- Oswald AMM, Reyes AD. Development of inhibitory timescales in auditory cortex. Cerebral Cortex. 2011; 21(6):1351–1361. https://doi.org/10.1093/cercor/bhq214 PMID: 21068186
- Levy RB, Reyes AD. Spatial profile of excitatory and inhibitory synaptic connectivity in mouse primary auditory cortex. Journal of Neuroscience. 2012; 32(16):5609–5619. https://doi.org/10.1523/JNEUROSCI.5158-11.2012 PMID: 22514322
- Rossi LF, Harris KD, Carandini M. Spatial connectivity matches direction selectivity in visual cortex.
 Nature. 2020; 588(7839):648–652. https://doi.org/10.1038/s41586-020-2894-4 PMID: 33177719

- Shi YL, Steinmetz NA, Moore T, Boahen K, Engel TA. Cortical state dynamics and selective attention define the spatial pattern of correlated variability in neocortex. Nature communications. 2022; 13(1):1– 15. https://doi.org/10.1038/s41467-021-27724-4 PMID: 35013259
- **32.** Keane A, Gong P. Propagating waves can explain irregular neural dynamics. Journal of Neuroscience. 2015; 35(4):1591–1605. https://doi.org/10.1523/JNEUROSCI.1669-14.2015 PMID: 25632135
- Pyle R, Rosenbaum R. Spatiotemporal dynamics and reliable computations in recurrent spiking neural networks. Physical Review Letters. 2017; 118(1):018103. https://doi.org/10.1103/PhysRevLett.118. 018103 PMID: 28106418
- Ermentrout GB, Cowan JD. A mathematical theory of visual hallucination patterns. Biological cybernetics. 1979; 34(3):137–150. https://doi.org/10.1007/BF00336965 PMID: 486593
- Rosenbaum R, Doiron B. Balanced networks of spiking neurons with spatially dependent recurrent connections. Physical Review X. 2014; 4(2):021039. https://doi.org/10.1103/PhysRevX.4.021039
- **36.** Avitabile D. Numerical computation of coherent structures in spatially-extended systems. In: Second International Conference on Mathematical Neuroscience, Antibes Juan-les-Pins; 2016.
- Ali R, Harris J, Ermentrout B. Pattern formation in oscillatory media without lateral inhibition. Physical Review E. 2016; 94(1):012412. https://doi.org/10.1103/PhysRevE.94.012412 PMID: 27575169
- **38.** Teschl G. Ordinary differential equations and dynamical systems. vol. 140. American Mathematical Soc.; 2012.
- Wolf A, Swift JB, Swinney HL, Vastano JA. Determining Lyapunov exponents from a time series. Physica D: nonlinear phenomena. 1985; 16(3):285–317. https://doi.org/10.1016/0167-2789(85)90011-9
- Mariño J, Schummers J, Lyon DC, Schwabe L, Beck O, Wiesing P, et al. Invariant computations in local cortical networks with balanced excitation and inhibition. Nature neuroscience. 2005; 8(2):194. https://doi.org/10.1038/nn1391 PMID: 15665876
- Geiger JR, Lübke J, Roth A, Frotscher M, Jonas P. Submillisecond AMPA receptor-mediated signaling at a principal neuron-interneuron synapse. Neuron. 1997; 18(6):1009–1023. https://doi.org/10.1016/ S0896-6273(00)80339-6 PMID: 9208867
- **42.** Xiang Z, Huguenard JR, Prince DA. GABAA receptor-mediated currents in interneurons and pyramidal cells of rat visual cortex. The Journal of Physiology. 1998; 506(3):715–730. https://doi.org/10.1111/j. 1469-7793.1998.715bv.x PMID: 9503333
- Cross MC, Hohenberg PC. Pattern formation outside of equilibrium. Reviews of modern physics. 1993; 65(3):851. https://doi.org/10.1103/RevModPhys.65.851
- Nauhaus I, Busse L, Carandini M, Ringach DL. Stimulus contrast modulates functional connectivity in visual cortex. Nature neuroscience. 2009; 12(1):70. https://doi.org/10.1038/nn.2232 PMID: 19029885
- 45. Smith GB, Hein B, Whitney DE, Fitzpatrick D, Kaschube M. Distributed network interactions and their emergence in developing neocortex. Nature neuroscience. 2018; 21(11):1600–1608. https://doi.org/10.1038/s41593-018-0247-5 PMID: 30349107
- **46.** Yu Y, Stirman JN, Dorsett CR, Smith SL. Mesoscale correlation structure with single cell resolution during visual coding. BioRxiv. 2019; p. 469114.
- Pinto L, Dan Y. Cell-type-specific activity in prefrontal cortex during goal-directed behavior. Neuron. 2015; 87(2):437–450. https://doi.org/10.1016/j.neuron.2015.06.021 PMID: 26143660
- Rothschild G, Nelken I, Mizrahi A. Functional organization and population dynamics in the mouse primary auditory cortex. Nature neuroscience. 2010; 13(3):353–360. https://doi.org/10.1038/nn.2484
 PMID: 20118927
- Henrie JA, Shapley R. LFP power spectra in V1 cortex: the graded effect of stimulus contrast. Journal of neurophysiology. 2005; 94(1):479–490. https://doi.org/10.1152/jn.00919.2004 PMID: 15703230
- Ray S, Maunsell JH. Differences in gamma frequencies across visual cortex restrict their possible use in computation. Neuron. 2010; 67(5):885–896. https://doi.org/10.1016/j.neuron.2010.08.004 PMID: 20826318
- Okun M, Steinmetz NA, Lak A, Dervinis M, Harris KD. Distinct structure of cortical population activity on fast and infraslow timescales. Cerebral Cortex. 2019; 29(5):2196–2210. https://doi.org/10.1093/cercor/bbz023 PMID: 30796825
- Bak P, Tang C, Wiesenfeld K. Self-organized criticality: An explanation of the 1/f noise. Physical review letters. 1987; 59(4):381. https://doi.org/10.1103/PhysRevLett.59.381 PMID: 10035754
- 53. Beggs JM, Plenz D. Neuronal avalanches in neocortical circuits. Journal of neuroscience. 2003; 23 (35):11167–11177. https://doi.org/10.1523/JNEUROSCI.23-35-11167.2003 PMID: 14657176
- 54. Bedard C, Kroeger H, Destexhe A. Does the 1/f frequency scaling of brain signals reflect self-organized critical states? Physical review letters. 2006; 97(11):118102. https://doi.org/10.1103/PhysRevLett.97. 118102 PMID: 17025932

- Touboul J, Destexhe A. Can power-law scaling and neuronal avalanches arise from stochastic dynamics? PloS one. 2010; 5(2):e8982. https://doi.org/10.1371/journal.pone.0008982 PMID: 20161798
- Engelken R, Wolf F, Abbott L. Lyapunov spectra of chaotic recurrent neural networks. arXiv preprint arXiv:200602427. 2020.
- De La Rocha J, Doiron B, Shea-Brown E, Josić K, Reyes A. Correlation between neural spike trains increases with firing rate. Nature. 2007; 448(7155):802–806. https://doi.org/10.1038/nature06028
- Kanashiro T, Ocker GK, Cohen MR, Doiron B. Attentional modulation of neuronal variability in circuit models of cortex. Elife. 2017; 6:e23978. https://doi.org/10.7554/eLife.23978 PMID: 28590902
- 59. Jan YI. Équilibre statistique pour les produits de difféomorphismes aléatoires indépendants. In: Annales de l'IHP Probabilités et statistiques. vol. 23; 1987. p. 111–120.
- 60. Baxendale PH. Stability and equilibrium properties of stochastic flows of diffeomorphisms. In: Diffusion Processes and Related Problems in Analysis, Volume II. Springer; 1992. p. 3–35.
- Kohn A, Coen-Cagli R, Kanitscheider I, Pouget A. Correlations and neuronal population information. Annual review of neuroscience. 2016; 39:237–256. https://doi.org/10.1146/annurev-neuro-070815-013851 PMID: 27145916
- 62. Horvát S, Gămănuţ R, Ercsey-Ravasz M, Magrou L, Gămănuţ B, Van Essen DC, et al. Spatial embedding and wiring cost constrain the functional layout of the cortical network of rodents and primates. PLoS biology. 2016; 14(7):e1002512. https://doi.org/10.1371/journal.pbio.1002512 PMID: 27441598
- Finn IM, Priebe NJ, Ferster D. The emergence of contrast-invariant orientation tuning in simple cells of cat visual cortex. Neuron. 2007; 54(1):137–152. https://doi.org/10.1016/j.neuron.2007.02.029 PMID: 17408583
- Rubin DB, Van Hooser SD, Miller KD. The stabilized supralinear network: a unifying circuit motif underlying multi-input integration in sensory cortex. Neuron. 2015; 85(2):402–417. https://doi.org/10.1016/j.neuron.2014.12.026 PMID: 25611511
- 65. Miller KD, Troyer TW. Neural noise can explain expansive, power-law nonlinearities in neural response functions. Journal of neurophysiology. 2002; 87(2):653–659. https://doi.org/10.1152/jn.00425.2001 PMID: 11826034
- 66. Hansel D, Van Vreeswijk C. How noise contributes to contrast invariance of orientation tuning in cat visual cortex. Journal of Neuroscience. 2002; 22(12):5118–5128. https://doi.org/10.1523/JNEUROSCI.22-12-05118.2002 PMID: 12077207
- Kadmon J, Sompolinsky H. Transition to chaos in random neuronal networks. Physical Review X. 2015; 5(4):041030. https://doi.org/10.1103/PhysRevX.5.041030
- **68.** Ostojic S. Two types of asynchronous activity in networks of excitatory and inhibitory spiking neurons. Nature neuroscience. 2014; 17(4):594–600. https://doi.org/10.1038/nn.3658 PMID: 24561997
- **69.** Schuecker J, Goedeke S, Helias M. Optimal sequence memory in driven random networks. Physical Review X. 2018; 8(4):041029. https://doi.org/10.1103/PhysRevX.8.041029
- Renart A, de La Rocha J, Bartho P, Hollender L, Parga N, Reyes A, et al. The asynchronous state in cortical circuits. Science. 2010; 327(5965):587–590. https://doi.org/10.1126/science.1179850 PMID: 20110507
- Molgedey L, Schuchhardt J, Schuster HG. Suppressing chaos in neural networks by noise. Physical review letters. 1992; 69(26):3717. https://doi.org/10.1103/PhysRevLett.69.3717 PMID: 10046895
- Lajoie G, Lin KK, Shea-Brown E. Chaos and reliability in balanced spiking networks with temporal drive. Physical Review E. 2013; 87(5):052901. https://doi.org/10.1103/PhysRevE.87.052901 PMID: 23767592
- 73. Kuramoto Y. Chemical oscillations, waves, and turbulence. Springer-Verlag Berlin Heidelberg; 1984.
- Steyn-Ross ML, Steyn-Ross DA, Sleigh JW. Interacting Turing-Hopf instabilities drive symmetry-breaking transitions in a mean-field model of the cortex: a mechanism for the slow oscillation. Physical Review X. 2013; 3(2):021005. https://doi.org/10.1103/PhysRevX.3.021005
- Destexhe A. Oscillations, complex spatiotemporal behavior, and information transport in networks of excitatory and inhibitory neurons. Physical Review E. 1994; 50(2):1594. https://doi.org/10.1103/PhysRevE.50.1594 PMID: 9962131
- Roxin A, Brunel N, Hansel D. Role of delays in shaping spatiotemporal dynamics of neuronal activity in large networks. Physical review letters. 2005; 94(23):238103. https://doi.org/10.1103/PhysRevLett.94.238103 PMID: 16090506
- Mastrogiuseppe F, Ostojic S. Linking connectivity, dynamics, and computations in low-rank recurrent neural networks. Neuron. 2018; 99(3):609–623. https://doi.org/10.1016/j.neuron.2018.07.003 PMID: 30057201

- 78. Landau ID, Sompolinsky H. Coherent chaos in a recurrent neural network with structured connectivity. PLoS computational biology. 2018; 14(12):e1006309. https://doi.org/10.1371/journal.pcbi.1006309 PMID: 30543634
- 79. Aljadeff J, Stern M, Sharpee T. Transition to chaos in random networks with cell-type-specific connectivity. Physical review letters. 2015; 114(8):088101. https://doi.org/10.1103/PhysRevLett.114.088101 PMID: 25768781
- Lukoševičius M, Jaeger H. Reservoir computing approaches to recurrent neural network training. Computer Science Review. 2009; 3(3):127–149. https://doi.org/10.1016/j.cosrev.2009.03.005
- Buonomano DV, Maass W. State-dependent computations: spatiotemporal processing in cortical networks. Nature Reviews Neuroscience. 2009; 10(2):113–125. https://doi.org/10.1038/nrn2558 PMID: 19145235
- 82. Schuessler F, Mastrogiuseppe F, Dubreuil A, Ostojic S, Barak O. The interplay between randomness and structure during learning in RNNs. Advances in Neural Information Processing Systems. 2020; 33.
- 83. Huang C, Doiron B. Once upon a (slow) time in the land of recurrent neuronal networks. . . . Current opinion in neurobiology. 2017; 46:31–38. https://doi.org/10.1016/j.conb.2017.07.003 PMID: 28756341